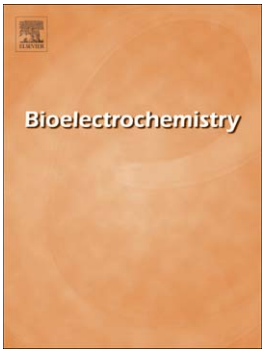

Interpulse multifrequency electrical impedance measurements during electroporation of adherent differentiated myotubes

Tomás García-Sánchez, Antoine Azan, Isabelle Leray, Javier Rosell-Ferrer, Ramon Bragós, LLuis M. Mir

PII: S1567-5394(15)00078-X
DOI: doi: 10.1016/j.bioelechem.2015.05.018
Reference: BIOJEC 6860

To appear in: *Bioelectrochemistry*

Received date: 12 December 2014
Revised date: 25 May 2015
Accepted date: 31 May 2015

Please cite this article as: Tomás García-Sánchez, Antoine Azan, Isabelle Leray, Javier Rosell-Ferrer, Ramon Bragós, LLuis M. Mir, Interpulse multifrequency electrical impedance measurements during electroporation of adherent differentiated myotubes, *Bioelectrochemistry* (2015), doi: 10.1016/j.bioelechem.2015.05.018

Interpulse multifrequency electrical impedance measurements during electroporation of adherent differentiated myotubes

Tomás García-Sánchez[a,*], Antoine Azan[b,c], Isabelle Leray[b,c], Javier Rosell-Ferrer[a], Ramon Bragós[a], LLuis M. Mir[b,c,*]

[a] *Electronic and Biomedical Instrumentation Group, Department of Electronic Engineering, Universitat Politècnica de Catalunya, Barcelona, Spain*
[b] *CNRS, UMR8203 Vectorologie et thérapeutiques anti-cancéreuses, Institut Gustave-Roussy, Villejuif, France*
[c] *Univ. Paris-Sud, UMR8203, Orsay, France*

Abstract

In this study, electrical impedance spectroscopy measurements are performed during electroporation of monolayers of differentiated myotubes. The time resolution of the system (1 spectrum/ms) enable 860 full spectra (21 frequencies from 5 kHz to 1.3 MHz) to be acquired during the time gap between consecutive pulses (interpulse) of a classical electroporation treatment (8 pulses, 100 μs, 1 Hz). Additionally, the characteristics of the custom microelectrode assembly used allow the experiments to be performed directly *in situ* in standard 24 multi-well plates. The impedance response dynamics are studied for three different electric field intensities (400, 800 and 1200 V/cm). The multifrequency information, analysed with the Cole model, reveals a short-term impedance recovery after each pulse in accordance with the fast resealing of the cell membrane, and a long-term impedance decay over the complete treatment in accordance with an accumulated effect pulse after pulse. The analysis shows differences between the lowest electric field condition and the other two, suggesting that different mechanisms that may be related with the reversibility of the process are activated. As a result of the multifrequency information, the system is able to measure simultaneously the conductivity variations due to ion diffusion during electroporation. Finally, in order to reinforce the physical interpretation of the results, a complementary electrical equivalent model is used.

Keywords: Electroporation, Electrical impedance spectroscopy, Adherent cells, Cole model, Electrical model

*Corresponding authors
Email addresses: tomas.garcia.sanchez@upc.edu (Tomás García-Sánchez), Luis.MIR@gustaveroussy.fr (LLuis M. Mir)

1. Introduction

The plasma membrane of living cells constitutes the barrier between the intracellular and extracellular media and regulates the transport of chemical species from or into the cell cytoplasm. Electroporation, also called electropermeabilization, is a phenomenon that occurs when cell membranes are exposed to high electric field pulses. When the parameters of such an electric field are appropriate, a transient state of permeability to molecular species is generated [1]. This technique is currently used as a tool to deliver membrane-impermeable molecules into the cells, both *in vitro* and *in vivo*, with its main interest focused on electrochemotherapy of tumors and gene electrotransfer [2–5]. When the electric field parameters exceed a certain threshold, the state of membrane permeability becomes permanent, thus leading to cell death. This phenomenon, known as irreversible electroporation, is currently used in nonthermal tissue ablation procedures [6] or as a sterilization method in food industry applications [7], among others.

The accumulated experimental evidence about the technique and the deep understanding of the effects of different parameters on the efficacy of the treatments have led to an increasingly widespread use of electroporation. For instance, in recent years the number of patients treated for local tumors with electrochemotherapy has increased considerably [5]. However, from a molecular point of view, there is no definitive explanation of the underlying mechanisms that govern the structural changes in the membrane during electroporation [1]. The most widely accepted theoretical description, which better describes membrane permeabilization, is the formation of aqueous pores in the lipid bilayer [8].

The creation of these pores has been the object of study using a variety of approaches, from molecular simulations [9] to the observation of artificial lipid membranes and measurements on real systems. Standard methods employed to assess the creation of pores imply molecular reporters and imaging techniques to measure molecular transport across the membrane. If the focus is placed on the kinetics of pore formation and resealing, fast dynamical methods are necessary due to the transient behaviour of some of the membrane permeable structures within a range of milliseconds [10]. Some attempts have been made using chemical methods in combination with fast optical techniques [11–13]. Measurements of the electrical properties of the membrane during pulse application have also been used to reveal the tempo-

ral evolution of pores by previous authors [10, 14]. An abrupt change in the electrical conductivity of the cell membrane in response to pulse application has been observed in individual cells [15, 16], cell suspensions [14, 17, 18] or tissues[19, 20]. Electrical measurements have usually been performed by observing the changes in the applied current-voltage waveform, which mainly consist of quasi-dc conductivity changes. Other attempts have used AC signals to study the passive electrical properties of the sample before and after electroporation at single frequencies [21–23]. Only in a few studies have multifrequency measurements been performed, also referred to as electrical impedance spectroscopy (EIS), on electroporated samples [20, 24, 25]. For example, Ivorra et al. [20] took measurements in a tumor tissue model using two frequencies in the interval between pulses (1 kHz and 15.5 kHz at a rate of 500 samples per second) and multifrequency measurements (an 11-frequency sweep from 1 kHz to 400 kHz) after pulse application. However, traditional EIS approaches based on frequency sweeps are not feasible for monitoring the fast dynamical changes in the membrane during pulse application due to the long measuring time needed when compared with the short interpulse period (usually $\leqslant$ 1 s). Broadband signals such as binary [26], chirp or multisine excitations [27] have previously been proposed to study fast dynamical phenomena with EIS. Other attempts to study fast pore dynamics are based in time domain methods such as time-domain reflectometry [28] or time-domain dielectric spectroscopy [18]. In this work, a multisine-based approach [29] is used to perform for the first time fast EIS measurements (1 spectrum per millisecond) during the interpulse electroporation interval, with the aim of studying pore creation and resealing dynamics.

Traditional *in vitro* electroporation cuvette setups require cells to be suspended during pulse application and are not suitable for treatment of anchorage-dependent cells. However, in some cases it is mandatory to preserve the state of adherence of the cell monolayer during pulse application. This is the case of neuronal cell cultures, differentiated cells, induced pluripotent stem cells (IPSc), etc.. Different approaches have been used to perform electroporation on adherent cells [30]. In the present study, experiments are performed in monolayers of differentiated myotubes using the system previously reported in [31], which is specifically conceived to apply *in situ* electroporation to adherent cells in standard multiwell culture plates. The interest of using differentiated cells *in vitro* is based on the fact that they describe more realistic models to study different aspects that could be trans-

lated into the clinical applications. For example, in the case of muscle tissue, the potential interest has been shown by using electroporation as a tool for electrogenetherapy *in vivo* [32] and how a real-time control system would be desirable for safe and efficient gene transfer [33]. The goal of this study is to test the suitability of the proposed microelectrode assembly in conjunction with the multisine-based approach to characterize and better understand the fast changes produced in the cell membrane during pulse application.

2. Materials and Methods

2.1. Measurement setup

2.1.1. Reference signal

From all broadband excitation signals proposed in bioimpedance measurements, we used multisine excitation based on previous studies developed by our group (the reader is referred to the work by Sánchez et al. for furher details [29]). Summarizing, the multisine burst consisted of 21 frequencies following a Bilateral Quasi-Logarithmic (BQL) distribution from 5 kHz to 1.313 MHz that was designed to concentrate a higher number of frequencies around the impedance relaxation central frequency and to minimize the intermodulation products at the selected frequencies, thereby increasing the Signal to Noise Ratio (SNR) and reducing the injected energy to the system [34].

2.1.2. Hardware

The measurement system was built in an NI PXIe-1062Q chassis from National Instruments. The system included an embedded dualcore controller PXIe-8130. The reference signal was generated by an NI PXIe-5122 arbitrary waveform generator (200 MS/s, 16-bit), voltage and current response were acquired, filtered with anti-Alias filters (1.5 MHz) and digitized at 20 MHz sample rate with a two-channel high-speed digitizer card PXIe-5122 (100 MS/s, 14-bit). A custom built analog front-end was used to interface the microelectrodes and the measurement hardware. Specifically, the measuring reference signal (0.5 V) was injected into the sample through a precision resistor of 1 kOhm (measuring current $\leqslant$ 500 μA). The voltage sensing terminals were buffered with two high input impedance wideband operational

amplifiers (AD8066), and the difference between them was then amplified with a differential line receiver (MAX4145). The current was measured after conversion to voltage through a transimpedance amplifier based on the operational amplifier AD8066.

Additionally, the NI PXI-2530 high-density multiconfiguration multiplexer-matrix was used for controlling connections between the pulse generator, the measurement system and the microelectrodes. Commutation between electroporation or measurement connections was synchronously performed with a hardware-based trigger signal provided at the beginning of each pulse by the custom-built pulse generator employed. A block diagram of the complete system is depicted in Schematic 1a.

The sequence of electroporation/measurements began with 100 continuous initial pre-electroporation measurements (100 ms). Subsequently, the microelectrodes were connected to the pulse delivery equipment and the pulse generation was initiated (8 biphasic pulses, duration 100 μs positive + 100 μs delay + 100 μs negative, frequency 1 Hz). When the trigger signal from the pulse generator was detected by the PXI-2530 system, the connections were switched to the measuring system after a fixed delay of 15 ms. Subsequently, 860 multisine bursts were continuously generated and acquired. The connections were again immediately switched to the pulse generator and the system waited for the next pulse (125 ms). The sequence was repeated until completing the 8 pulses. The sequence of electroporation and measurement signals is detailed in Schematic 1b. The complete system was controlled by a custom software in Labview (National Instruments).

2.2. Microelectrodes

The microelectrode assembly used in this study was specifically designed to perform electroporation to adherent cell monolayers cultured in standard 24 multiwell plates. Details of the microelectrode concept, the fabrication procedure and some experimental results can be found in [31]. Summarizing, the microelectrodes consisted of Printed Circuit Board (PCB) discs (15 mm diameter), comprising six equally spaced lines coiled in parallel around the centre of the disc and forming six parallel spirals. The dimensions of the lines were 75 μm in width and 150 μm spacing between them. The microelectrode was designed to be positioned momentarily above the cell monolayer during electroporation/measurements procedure. In order to prevent direct contact

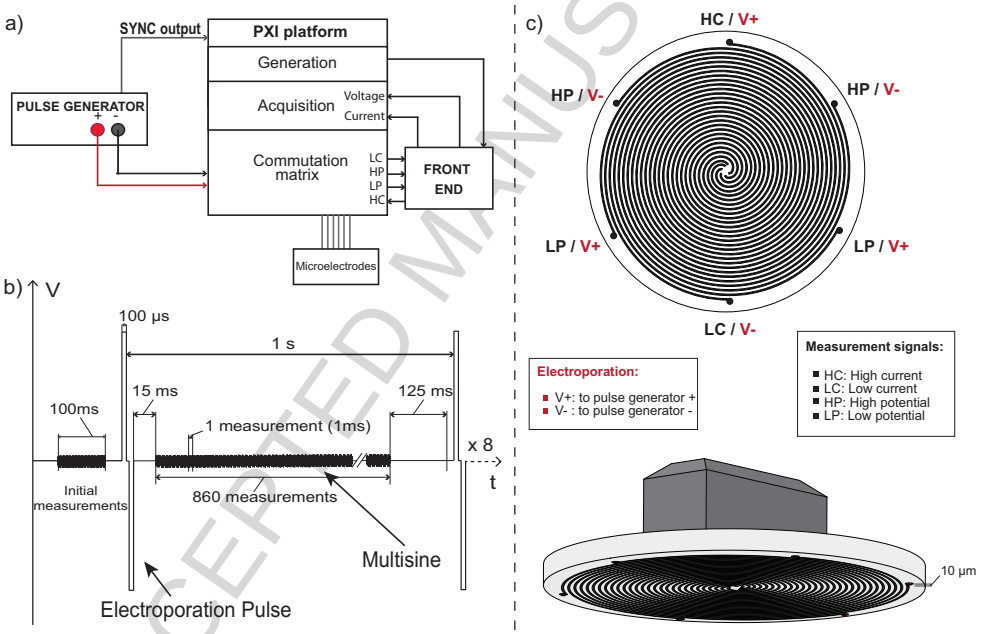

Schematic 1: Representation of the measurement setup and the microelectrodes. a) Measurement system block diagram. b) The sequence of electroporation and measurement signal. c) The spiral microelectrode topology and its connections.

between cells and electrodes, six microseparators with a thickness of 10 μm were patterned with an additional layer of photosensible epoxy on the external end of each spiral line. A schematic representation of the microelectrode topology and connections is depicted in Schematic 1c.

Furthermore, electrode topology was specially conceived to perform bioimpedance measurements with a four-electrode configuration. Four-electrode measuring configurations are suitable for reducing the effects of the electrode polarization caused by the electrode-electrolyte interface [35], consequently improving the ability of the system to detect changes related to the cells [36, 37]. In the present setup, we used a modified arrangement of a four-electrode measuring configuration by duplicating potential measurement terminals HP and LP (see Schematic 1c). This modification allows the whole area covered by the microelectrodes to be used as the measuring area, and is thus not sensitive to local changes but to the average variations in the cell monolayer.

2.3. Data pre-processing

The bioimpedance was estimated by measuring and processing an integer number of periods of the sample current and voltage response. The impedance was calculated on the basis of the division of the output-input Fast Fourier Transform (FFT) coefficients at the excited frequencies [38]. Once the impedance was calculated, noise reduction was performed with a moving average filter (length n=10) independently for each 860 ms continuous measurement segment.

Compensation for the effects of the system frequency response produced by the microelectrodes, cables, amplifiers, etc., was achieved by means of a three-reference calibration method [39]. The references were obtained by measuring, with the same setup, saline solutions with different conductivities (approx 0.1 $\pm$ 70 % S/m).

2.4. Cells and chemicals

C2C12 myoblasts were seeded into 24 multi-well plates at an initial density of $15{\times}10^3$ cells/well with 1 ml of growth medium comprising Dulbecco's Modified Eagle's Medium (DMEM; High Glucose, GlutaMAX^{TM} Supplement, pyruvate. Life technologies, Saint Aubin, France) supplemented with 10% fetal bovine serum (FBS) and 1% penicillin-streptomycin. The cells

were kept in an incubator at 37° under a 5% CO_2 atmosphere for 36-48 hours until the confluence was approximately 80-90%. Subsequently, the cells were rinsed once with PBS and once with DMEM, and the medium was then switched to 500 μl of differentiation medium consisting of DMEM supplemented with 2% FBS (Gibco, Carlsbad, CA, USA). After five days of differentiation, the cells were used for electroporation experiments.

A low-conductivity electroporation (LCE) buffer was used during the electroporation pulse delivery and impedance measurements. It consisted of 250 mM sucrose, 10 mM Tris and 1 mM $MgCl_2$ (pH 7, osmolarity 287 mmol/kg, conductivity 0.1 S/m).

Finally, as a permeabilization reporter, fluorescent nucleic acids stain Yo-Pro-1 Iodide (λ_{ex}=491 nm, λ_{em}=509 nm, Life technologies, Saint Aubin, France) was added to the permeabilization buffer at a final concentration of 1 μM.

2.5. Experimental procedure

To conduct the experiments, the cells were removed from the incubator and washed once with LCE buffer. Subsequently, 200 μl LCE + Yo-Pro (1 μM) were added. The cells were then introduced into a controlled temperature chamber at 37° C and left to stabilize for 10 minutes before pulse application. The complete experiment was performed in this controlled temperature environment. After this period, the microelectrode assembly was manually positioned above the cell monolayer by means of a custom-built applicator. Prior to their positioning above the cell monolayers, electrodes were wetted in LCE buffer. Immediately after, the Labview software which controls the whole system initiated the electroporation-measurement sequence described above. Once the sequence was finished, the microelectrodes were carefully removed and the cells were left for and additional 15 minutes for resealing. The cells were then washed twice with PBS and a fresh culture medium was added before inspection under the inverted microscope Zeiss Axio Observer Z1 (Carl Zeiss, Jena, Germany) to detect Yo-Pro fluorescence.

3. Results and Discussion

In this section, the most relevant findings resulting from the measurements are presented and discussed. First, an illustrative example of measurements performed in a cell monolayer and in a cell-free culture plate are compared in order to show the effects of the measurement system on the total impedance recorded. Once assessed, a mathematical compensation is proposed to reduce these effects. Data modelling is subsequently used to extract full information from the impedance response of cells during electroporation. First, the Cole model is used and a deep analysis on some of its parameters is presented for different electric field intensities. Finally, an equivalent electrical circuit is used to improve the understanding of the different effects observed in the measurements and to confirm some assumptions made during the analysis.

3.1. Cell monolayer vs. cell free measurements: illustrative example

3.1.1. Comparison

During the course of the experiments, negative controls were performed in the absence of cells, the same conditions being reproduced as in the case of measurements with cells. These tests were performed in order to study the impact of some possible undesired effects, mainly electrode polarization impedance (EPI) changes, temperature variations, etc.. In Fig. 1 the evolution of the real and imaginary part during the course of a single experiment is depicted for the same electric field (1200 V/cm, E=V/d with V=18 V and d=150 μm) applied to a cell monolayer and to a cell-free culture plate, both containing the same LCE buffer. The reader should be aware from now on that although measurements pulse after pulse are plotted continuously there is a delay between the end of an interpulse measurement and the beginning of the next one. Results are shown for five different frequencies corresponding to the lower band of each spectrum, where the impact of both cell membrane permeabilization and electrode polarization is maximum [40, 41].

The differences observed between both cases clearly demonstrates that the measuring setup is sensitive to the detection of the impedance changes produced in the cell membrane during electroporation, and that these changes predominate over other undesired effects. Among these effects, the most likely explanation for the small changes observed in the absence of cells is

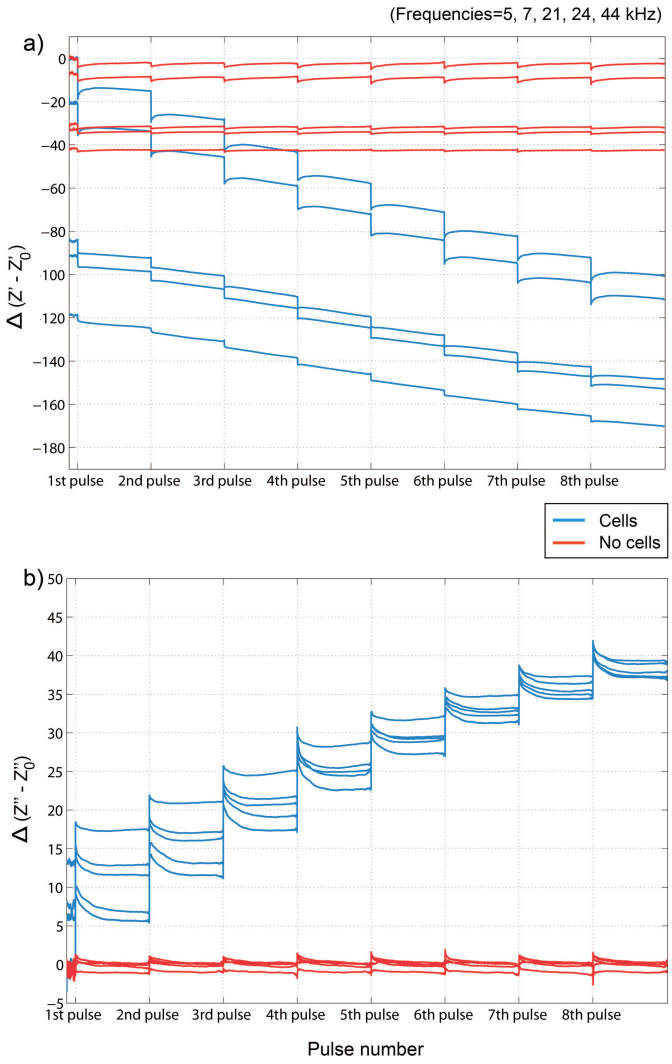

Figure 1: Comparison of interpulse impedance evolution (real and imaginary part) for an electric field of 1200 V/cm (E=V/d, with V=18 V and d=150 μm) applied to a myotubes monolayer in blue (cells) and to a cell-free culture plate in red (No cells) with the same extracellular buffer. The evolution at frequencies of 5, 7, 21, 24 and 44 kHz is presented normalized with respect to the impedance measured at f= 5 kHz for time t=0 (Z_0).

the transient variation of EPI in response to the application of high electric field pulses.

When the electroporation pulses are applied to the metal microelectrodes immersed in the electrolytic buffer, the system is displaced from its equilibrium due to the temporal disruption of the electrode-electrolyte double layer [41–43]. The redistribution of charges is then immediately able to follow an exponential behaviour in order to reach equilibrium again [44]. The perturbation of this effect on the measurements should be minimized because of two main causes; i) the application of bipolar EP pulses, which minimizes the reactions in the electrode-electrolyte interface, as a consequence of the reduction of the net charge transfer during pulse application [45], and ii) the four-electrode measuring strategy mentioned above. However, these strategies are unable to eliminate this completely.

3.1.2. Compensation

Although the observed effect of the system on the measurements is very small in comparison to the changes detected in the presence of cells, it is still desirable to perform some kind of compensation in order to obtain more accurate information about the impedance evolution during cell membrane electroporation.

First, we make the assumption that the EPI behaves identically in response to the application of pulses of a fixed electric field intensity, either in the absence or presence of cells. This is supported by the fact that there is no direct contact between cells and electrodes, which could significantly modify the current density through them. Moreover, multiple tests performed in a cell-free plate with the same microelectrode assembly before and after experiments with cells resulted in very similar behaviour (data not shown). Secondly, according to the basic equivalent circuits used to model the electrode-electrolyte interface, the EPI is represented in series with the sample under test [41, 46, 47]. Thus, the EPI variation may be regarded as an additive effect in the total impedance (see Schematic 2).

Based on these assumptions, we are able to state that the temporal evolution of measured impedance in the presence of cells is the sum of two terms, and it is possible to subtract the normalized temporal evolution of the measurements without cells to determine the behaviour of the cells alone (see Equations 1 - 3). As the response of the EPI depends both on the applied

electric field and the measured frequency, the subtraction is performed for each individual frequency and electric field intensity. Henceforth, all the measurements appearing in this work have been compensated for this effect.

$$Z_{cells}(\omega, t, E) = Z_{Electroporation}(\omega, t, E) + Z_{EPI}(\omega, t, E) \tag{1}$$

$$Z_{NOcells}(\omega, t, E) = Z_{EPI}(\omega, t, E) \tag{2}$$

$$Z_{Electroporation}(\omega_k, t, E_k) = Z_{cells}(\omega_k, t, E_k) - Z_{NOcells}(\omega_k, t, E_k) \tag{3}$$

3.2. Data modelling

One of the main advantages of acquiring complete spectral information instead of single frequency measurements from the system under study is the possibility of using models to better understand and predict the behaviour of these systems. In the present work, we use two models to study the evolution of impedance during electroporation of a cell monolayer. First of all, we use the widely known Cole model and subsequently introduce a more complex equivalent circuit (see Schematic 2).

The Cole model may be fully described by four parameters: R_0 represents the resistances at very low frequency; R_∞ accounts for the resistance at very high frequency; α is the exponent of the CPE in the model, and τ_c is the characteristic relaxation time constant of the circuit. One of the main advantages of using Cole model instead of more sophisticated models is that, due to its simplicity, the parameter calculation process is more efficient in terms of computational costs, which is valuable for real-time systems where parameter analysis should be done online [48].

The electrical equivalent model proposed in this study is shown in Schematic 2c. It corresponds to the simple version of a 2R-1C circuit augmented by a resistor in parallel with the membrane capacitance proposed by Fricke and Morse [49] to simulate the conducting state of the membrane. The only difference is that in the circuit presented here, the capacitance is replaced

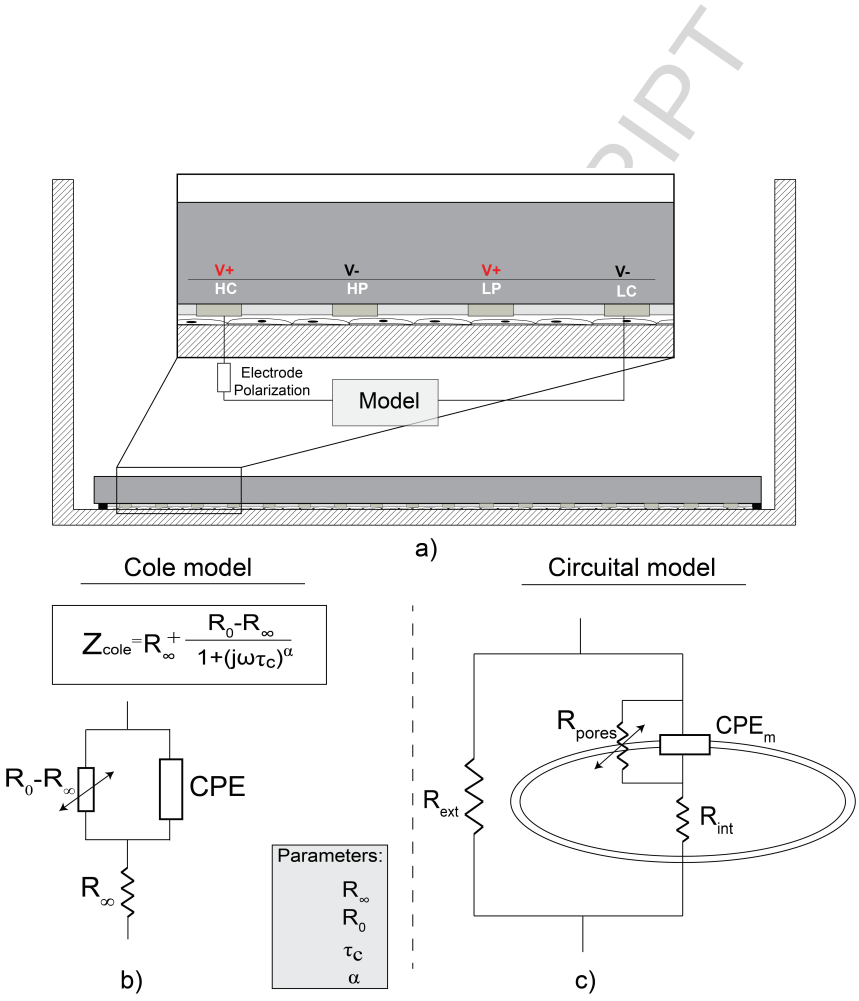

Schematic 2: Representation of the cell-electrode system. a) Schematic view of the geometry is shown; the Electrode Polarization Impedance (EPI) is represented in series with the cell model . b) and c) The Cole model and the proposed equivalent circuit are summarized respectively.

by a CPE (CPE_m), which more closely resembles the frequency-dependent behaviour of the membrane capacitor. Similar models have been used by previous authors to study the electrical properties of cells during electroporation [25, 50–53].

3.3. The Cole model

In an unaltered cell monolayer, the current at very low frequencies is blocked by the presence of cell membranes, while at high frequency, the current flows freely across the membrane. When the cell membrane is permeabilized as a consequence of electroporation, the previous situation is no longer valid. In an electroporated sample, the current at low frequencies can find new paths through membrane. In these conditions, R_0 should be significantly modified by the dynamics of pore formation and resealing while R_∞ should not be sensitive to the creation of pores in the membrane. The conductivity changes in the extracellular and intracellular resistances derived from ion leakage through membrane pores or volume variations should indirectly affect the values of both R_0 and R_∞.

In Fig. 2a (dots) the data and the corresponding adjusted Cole model (blue line) of the initial (pre-electroporation) monolayer impedance of a single experiment are plotted in a Wessel diagram. The measurements clearly describe a single dispersion arc compatible with the Cole model. Subsequently, all data sets (100 + 8x860) were adjusted to the model with a MATLAB routine. Fig. 2b shows the evolution of the Cole arcs during the complete electroporation treatment (E=1200 V/cm,8 pulses, 1 Hz) of the same sample. The temporal evolution of Cole model parameters R_0 and R_∞ is shown in Figs. 2c and d.

The observation of R_0 evolution reveals two different dynamic processes. First, a fast recovery of the impedance values in accordance with the resealing of plasma membrane immediately after each pulse application is detected (**short-term evolution**). Secondly, in accordance with the creation of more stable membrane pores, an accumulated impedance decay over time with slower behaviour is superimposed (**long-term evolution**). On the other hand, the evolution of R_∞ only reveals a maintained decay over time. Given that the appearance of pores in the membrane involves a great variation of the resistive current paths through membrane, represented by R_0 and R_∞, for conciseness, the analysis of the other two Cole parameters α and τ_c is

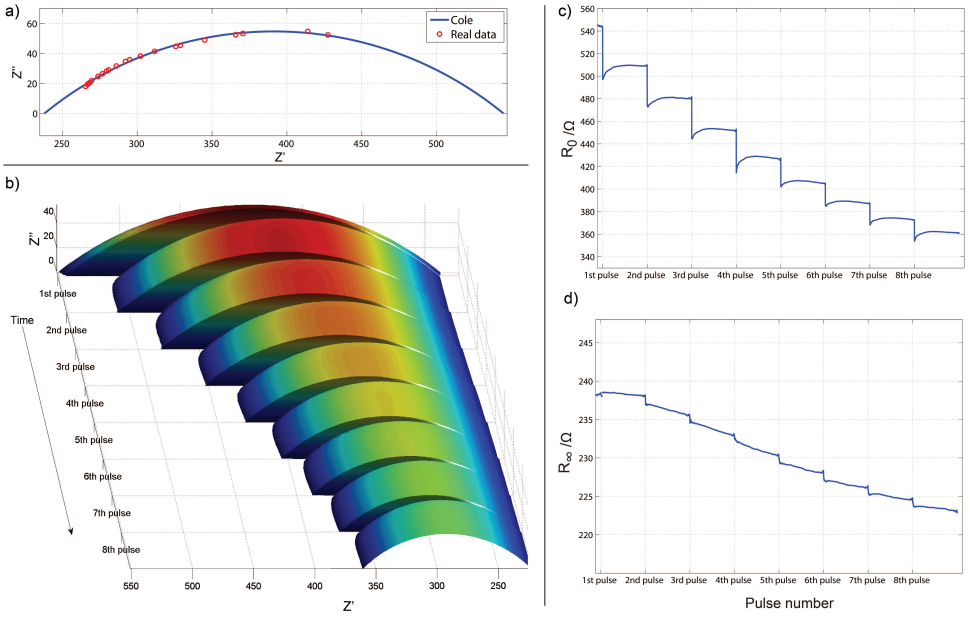

Figure 2: Example of adjusted data to the Cole model; a) Initial pre-electroporation state; the dots represent the real data, while the line corresponds to the adjusted model; b) plot of the temporal evolution of the adjusted Cole arcs for a single experiment applying E=1200 V/cm, 8 pulses and 1 Hz. Evolution of parameters R_0 and R_∞ for the same example are shown in c) and d).

omitted in this study. A detailed analysis for R_0 and R_∞ is given below.

3.3.1. Short-term analysis

We first focus on the transient impedance recovery observed in R_0. In order to make an independent analysis of this process, it is necessary to separate it from the superimposed long-term decay observed. Fig. 3a shows an illustrative example of the obtained long-term evolution (dashed lines) for each electric field condition. This component is then subtracted from the original data to obtain the corrected short-term information. The corrected mean value (± SD) of the short-term dynamics for at least three repetitions of each electric field is shown in Fig. 3b. The analysis of the fast impedance recovery after each pulse can now be studied independently.

A double exponential behaviour according to Equation 4 is proposed to follow this short-term impedance evolution. In order to determine a quantitative measure of the time constants for this dynamic evolution, the 8 fragments of measurements corresponding to each inter-pulse window are individually processed in MATLAB to obtain the values of the time constants τ_1 and τ_2.

$$f(t) = Ae^{-t/\tau_1}{}_{(Fast)} + Be^{-t/\tau_2}{}_{(Slow)} \tag{4}$$

Fig. 4a illustrates an example of the fitted double exponentials for the different electric field intensities. The term **fast** is used to describe the first part of the function, where there is a rapid variation. The second part shows a more gradual increase referred as **slow**.The evolution of the obtained time constants pulse after pulse is shown in Figs. 4b and c.

According to these results, the time constant (τ_1) shows no evolution during the course of the 8 electroporation pulses. This indicates that the dynamics of the mechanism responsible for pores resealing at this stage are stable over time. The mean value of τ_1 calculated as the average of the values obtained for the 8 inter-pulse fragments of each experiment are summarized in Fig. 5. The mean values differ considerably between the lowest electric field (400 V/cm), where τ_1 is approximately twice as big as the values obtained for the other two electric field intensities. As confirmed by fluorescent dye uptake, the case of 400 V/cm corresponds to the lower bound of permeabilization, while in the case of 800 V/cm and 1200 V/cm cells are extensively permeabilized. This may account for the differences observed.

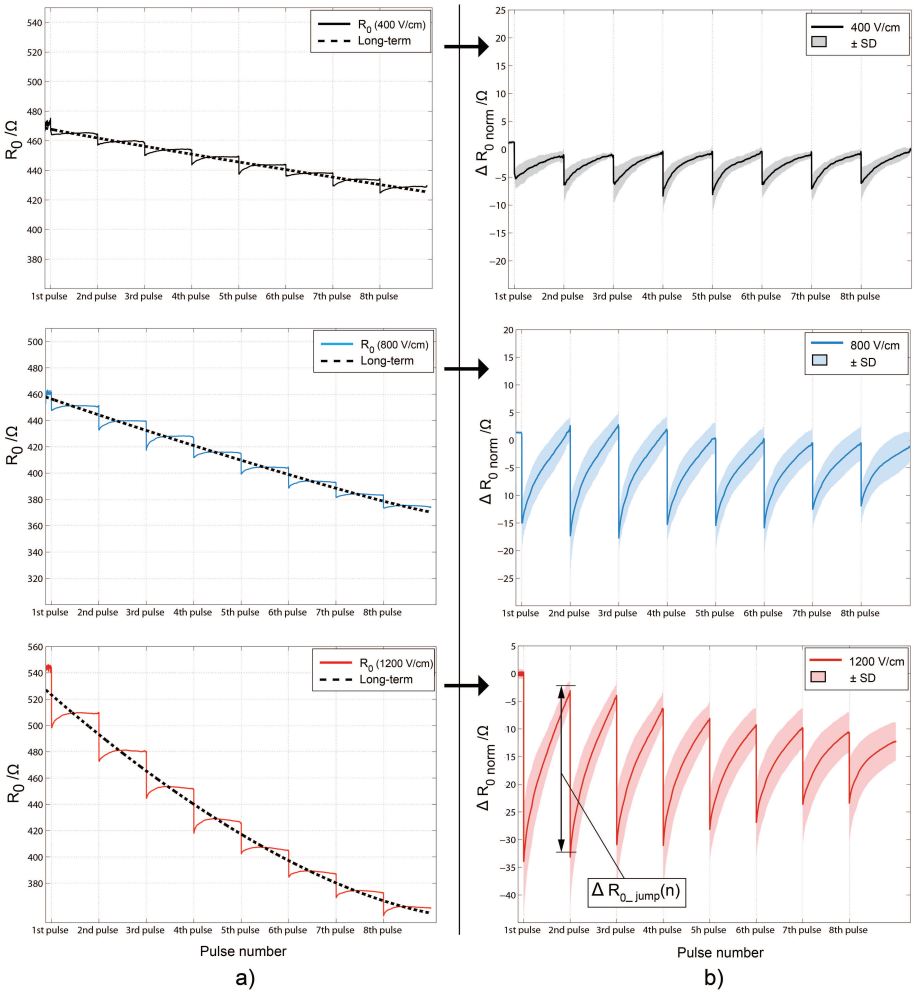

Figure 3: Analysis of parameter R_0. An illustrative example for each electric field condition is shown a) The complete evolution of R_0 (solid lines) and the corresponding fitted long-term impedance decay (dashed lines). b) The mean evolution of the corrected short-term dynamics after subtracting the long-term decay is shown. Mean values (± SD) are extracted from at least three repetitions for each electric field pooled together.

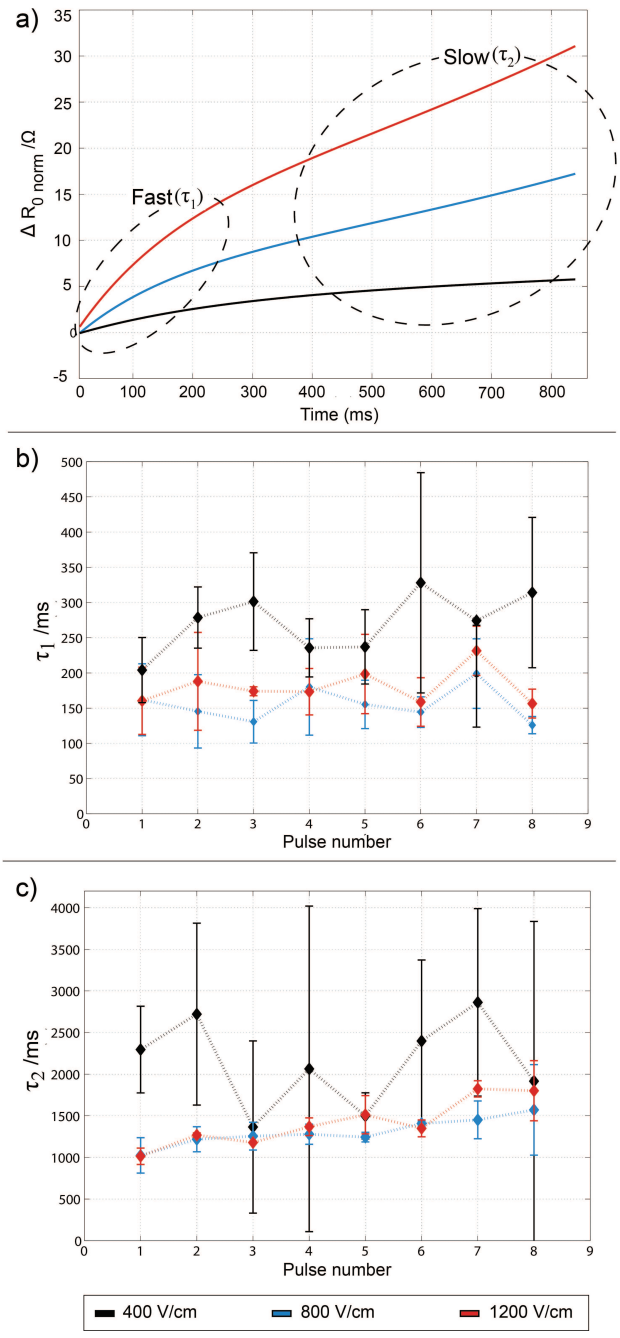

Figure 4: Double exponential short-term analysis. a) Example of the adjusted double exponential for the three different electric field intensities studied (400, 800 and 1200 V/cm). b) Evolution with pulse number of the mean time constant τ_1 for each electric field; error bars correspond to ± SD. c) Evolution with pulse number of the mean time constant τ_2 for each electric field; error bars correspond to ± SD. Values from at least three repetitions are pooled together.

Electric fields near to the threshold of permeabilization may not be enough to trigger the creation of large pores and only few small pores with a slower behaviour appear and fully reseal. Furthermore, the incomplete closure of pores as a result of a certain level of irreversibility in the case of 800 V/cm and 1200 V/cm, could also be a faster process than the time needed for the complete membrane repair produced with 400 V/cm.

With regard to the mean values of the slow time constant τ_2 shown in Fig. 5, there is again a significant difference between the lowest electric field and the other two. In this case, an increase in the value of τ_2 over time is observed for 800 and 1200 V/cm, while 400 V/cm shows no evolution. The time constant increases from around 1 s at the beginning of the treatment to more than 1.5 s at the end. The extension in the duration of this stage with increasing pulse number could be the consequence of a gradual loss in the resealing ability of cell membranes due to the accumulated effect of the pulse repetition. This may be because, as previously stated, for 800 V/cm and 1200 V/cm irreversible damage is produced in the cell membrane. The obtained values are in accordance with observations made previously by other authors who also measured durations of around one second for the total lifetime of the short-term membrane resealing mechanisms [21, 54–57].

These results highlight the fact that the process of membrane resealing is a complex mechanism in which several structures with different time constants evolve dynamically. In addition, according to a model proposed in [58], this short-term variation may be related to the conducting state of the membrane, while the long-term evolution that is analysed in the following section could be due to the state of permeability maintained in the membrane on a bigger time scale.

Finally, Fig. 6 depicts the evolution of the impedance drop immediately after the pulse, calculated as the difference between the value at the end of one inter-pulse measurement and the value at the beginning of the next one (see 3b, lower insert). It clearly shows an electric field dependence; increasing the impedance drop with higher electric fields. This supports the fact that the number (or size) of pores increases with field magnitude. Moreover, the decreasing value over time for 800 and 1200 V/cm can be accounted for by the reduction in the number of new pores created. This could be attributed to the fact that once the membrane is permeabilized, it is more difficult to reach again the transmembrane voltage threshold for electroporation, thus

reducing the ability of pore formation pulse after pulse.

3.3.2. Long-term analysis

The accumulated impedance decay corresponding to the long-term evolution observed in R_0 and R_∞ is analysed next. The data is obtained from fitting parameters R_0 (a) and R_∞ to double exponential functions in order to capture the asymptotic behaviour observed. The reader may refer to Fig. 3a (dashed lines) for an example of the long-term tendency obtained with R_0; a similar procedure is applied to R_∞. Fig. 7 shows the percentage of variation with respect to the initial pre-electroporation state of cell monolayers during the complete 8-pulse electroporation treatment.

Comparison of the evolution of both parameters shows that the relative percentage variation clearly differs between the low and high frequency resistances. In the case of the highest electric field (1200 V/cm), for example, parameter R_0 reduces to ≈70%, while R_∞ decreases to ≈93%. Furthermore, electric field dependence is also clearly observed in both parameters, the relative change being greater with increasing electric fields.

The differences in the relative percentage of variation observed between R_0 and R_∞ are explained by the fact that at least two events affecting the impedance recordings are occurring at the same time; first, the creation of pores in the membrane, and secondly, the change in conductivity of the extracellular and intracellular media caused by ion diffusion. Furthermore, volume variations caused by cell swelling could have an impact on the measurements. However, for the time scale considered, this effect can be neglected. In this situation, R_∞ should mainly be affected by the conductivity variations, while R_0 is affected by both conductivity and the changes produced in the plasma membrane.

Considering that R_∞ is determined by the parallel association of the intra and extracellular resistances, in order to explain the total decay observed, it is necessary to make the assumption that variation of the extracellular conductivity has a greater impact on the registered impedance. This assumption can be considered true as long as measurements are performed in a low-conductive buffer with conductivity several times lower than the intracellular space. Additionally, the spatial distribution of the components in the system can also help to explain this; a layer of extracellular medium exists between the electrodes and the cells (see Schematic 2). Therefore, the

Time Constant	400 V/cm	800 V/cm	1200 V/cm
Fast (τ_1)	271.6 ± 43 ms	155.3 ± 24.6 ms	180.1 ± 25.4 ms
	***		
	**		
			ns
Slow (τ_2)	2.14 ± 0.53 s	1.3 ± 0.16 s	1.41 ± 0.28 s
	**		
	*		
			ns
*** *p<0.0001*	** *p<0.001*	* *p<0.005*	ns: *non-significant statiscical difference*

Figure 5: Mean values (± SD) of the time constants for the double exponential functions corresponding to the short-term analysis of parameter R_0. Values from at least three repetitions are pooled together. The significance of differences in the unpaired Student́-test, p values are indicated in the figure footnotes.

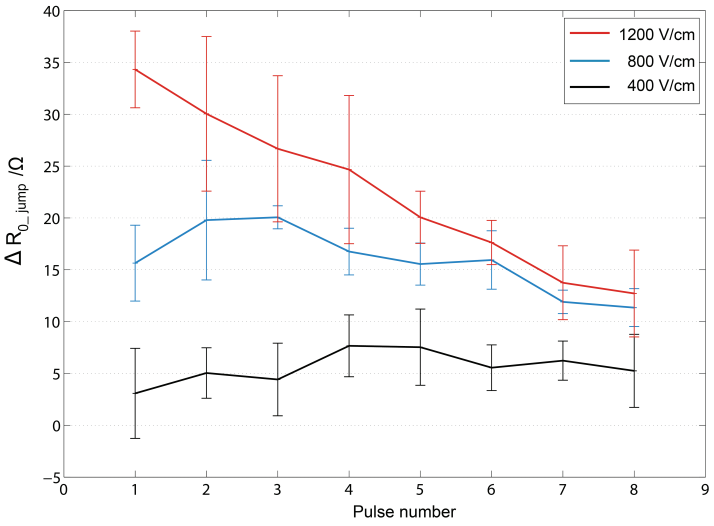

Figure 6: Evolution of the impedance drop immediately after each pulse for the different electric fields. Mean ± SD of at least three repetitions are pooled together.

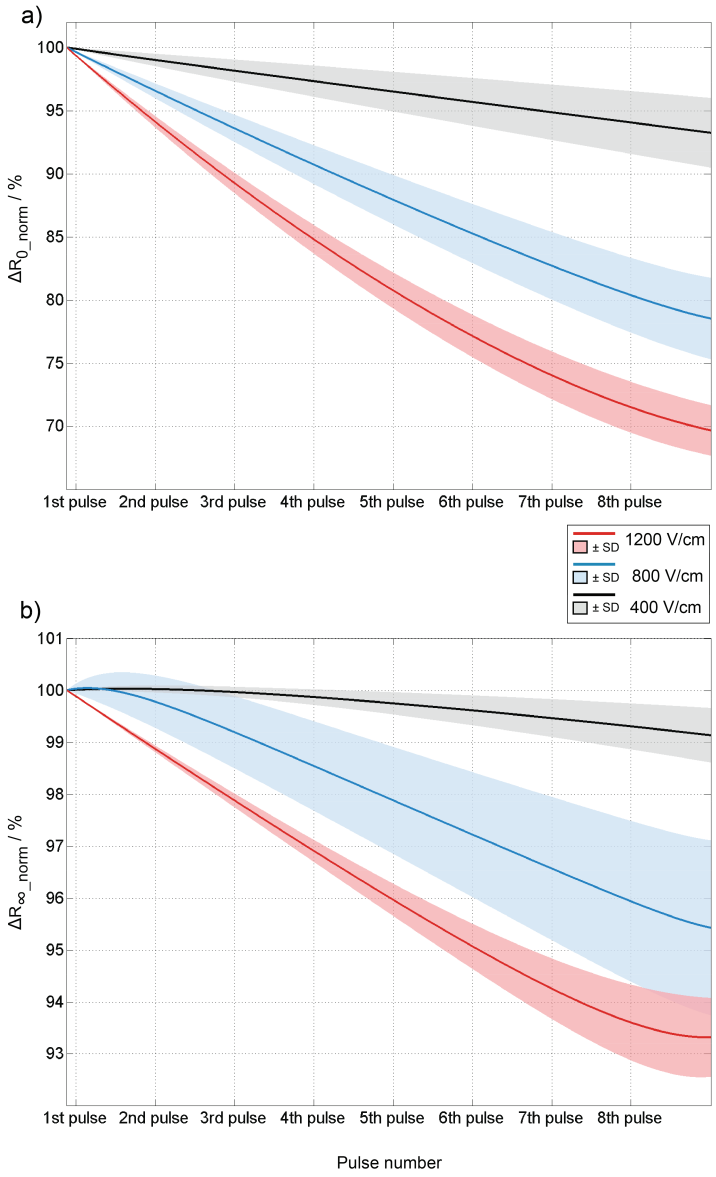

Figure 7: a) and b) Adjusted exponential for the long term decay of parameters R_0 and R_∞ respectively. Values are represented as the total normalized percentage of variation with respect to the initial pre-electroporation state. The shaded area corresponds to the standard deviation from at least three repetitions pooled together.

variation of R_∞ is explained by the release of ions from the cell to the extracellular medium attending to a diffusion mechanism in the range of several seconds [59]. The rate of this diffusion process is controlled, among other factors, by the amount of membrane pores and the concentration gradients, which explains why this process is not linear with the pulse number.

In the case of R_0, apart from the change in conductivity mentioned above, the long-term impedance decay accumulated is the result of the creation of more stable pores in the membrane that do not reseal in the time scale considered. These pores are believed to be ultimately responsible for the success, in terms of macromolecule uptake, of any electroporation treatment. From Fig. 7a it may be observed that R_0 follows an asymptotic behaviour, which suggests that the number of stable pores does not increase linearly with the pulse number, and there may exist a limit for new pore formation. This is in accordance with the fact that, from a certain level, increasing the number of pulses does not improve the effectiveness of the electroporation treatment [1, 60].

The analysis performed using the Cole model has shown how the information contained in R_0 can be used for analysing membrane variations in response to pulse application. However, the drawback of such a simple mathematical model is the fact that it does not include a specific parameter that accounts solely for membrane poration. As discussed above, the parameters R_0 and R_∞ are contributed by the intracellular and extracellular conductivity variations, and also by the membrane resistance changes. For this reason, it is not possible to analyse fully those effects independently and some assumptions have been made in the previous analysis. In the following section, a more complex equivalent circuit is proposed and used in order to confirm some of the previous assumptions.

3.4. Augmented electrical equivalent circuit

The aim of using an equivalent electrical model is to enable the behavior of the different parts of the system to be observed separately, and based on their physical meaning, to arrive at a correct interpretation of the measurements. The proposed electrical equivalent consists of the parameters R_{ext} and R_{int}, which correspond to the extracellular and intracellular resistances, respectively, and an additional resistance R_{pores} simulates the opening and closing of membrane pores (see Schematic 2c).

The analysis of the electrical equivalent is only shown for an illustrative example, which is valid for demonstrating the effectiveness of the model and its interpretation. The data corresponds to a single experiment applying 1200 V/cm; the same analysis was performed for the other conditions and shows a similar behaviour. First, the values for the initial pre-electroporation state are found manually in order to set the initial conditions to the fitting algorithm. Subsequently, circuit parameters are obtained automatically for each spectrum. During the course of the fitting procedure, it was noticed that there was more than one possible set of parameters solving the system. For this reason, some restrictions were imposed on the algorithm in accordance with the expected evolution of the parameters. Specifically, a lower bound was imposed for R_{int} corresponding to its initial pre-electroporation value, but no upper bound was imposed. Considering the release of ions from the cytoplasm, the decrease of R_{int} was unlikely to occur during the experiment. In addition, the α exponent is also forced not to increase; this condition is imposed by interpreting that lower values of α mean that the CPE tends to evince the behaviour of an ideal resistor, which seems reasonable after membrane poration.

In order to confirm that both models are compatible, the equivalent R_0 and R_∞ for the proposed circuit are calculated according to the following the equations:

$$R_0 = R_{ext}//(R_{int} + R_{pores}) \tag{5}$$

$$R_\infty = R_{ext}//R_{int} \tag{6}$$

Fig. 8a shows the initial fitted model and the corresponding measured data. In Figs. 8b and c, parameters R_0 and R_∞ from the two models are plotted together for the same set of measurements. It is clearly noticeable that the calculated parameters from the equivalent circuit lead to similar behaviour as those from the Cole model, thereby confirming the equivalence of both models.

Figs. 8d, e and f show the evolution of parameters R_{pores}, R_{ext} and R_{int}, respectively. The evolution of R_{pores} is in agreement with the behaviour observed in R_0, which confirms that the variations observed in this Cole model parameter are mainly modulated by the changes due to membrane

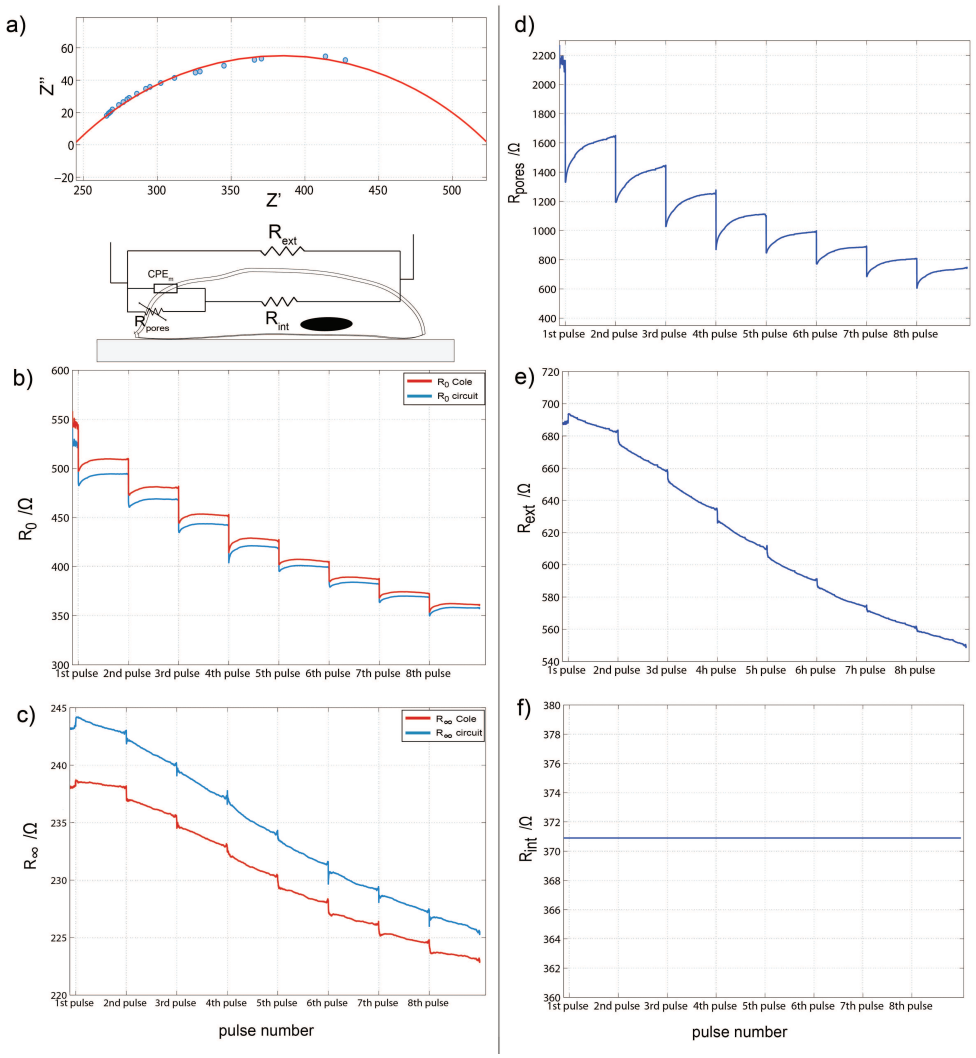

Figure 8: Adjusted equivalent circuit. a) Data and fitted arc for the initial pre-electroporation state of a single experiment applying 1200 V/cm. b) and c) Comparison of the calculated R_0 and R_∞ for the equivalent circuit and that obtained for the Cole model. d), e) and f) Evolution of parameters R_{pores}, R_{ext} and R_{int} of the equivalent circuit, respectively.

poration. In the case of R_{ext} (Fig. 8d), the extracted parameter shows a sustained slow decrease over time, while R_{int} shows a negligible increase. This is in agreement with the assumption that R_∞ from the Cole model is mainly influenced by the increase in the conductivity of the extracellular medium produced by the diffusion of ions. The previous observations validate the assumptions made during the analysis of the Cole model parameters, where R_0 is dominated by the membrane changes and R_∞ reflects the variation in the composition of the extracellular medium.

4. Conclusions

In this study, a fast EIS technique based on multisine excitations is used to measure impedance variations of differentiated myotube monolayers during electroporation. The time resolution of the system (1 spectrum/ms) enables multifrequency measurements to be made during the interpulse time window between consecutive pulses of a regular electroporation treatment. Additionally, the characteristics of the microelectrode assembly used allow the experiments to be conducted directly *in situ* with cells cultured in standard 24 multi-well plates.

In order to obtain a complete analysis of the multifrequency information, data sets are adjusted to the Cole impedance model. The analysis of parameter R_0 shows on the one hand a short-term impedance recovery in accordance to the membrane resealing events that occur up to 1 second after pulse application. The observed behaviour differs between the lowest electric field tested, which corresponds to the threshold for permeabilization, and the other two conditions, where cells are extensively permeabilized. On the other hand, a second long-term slow variation is observed in R_0 attributed to the accumulation of more stable pores in the membrane pulse after pulse. The increase in membrane permeability due to these pores is not linear with the pulse number and shows an asymptotic behaviour suggesting a limit for permeabilization with the pulse number.

The analysis of R_∞ shows a slow decrease, which reflects changes in the system that cannot be related to the cell membrane, but rather to other collateral effects such as the increase in the conductivity of the extracellular space caused by the diffusion of ions through membrane pores, volume variations due to cell swelling, etc..

Measurements are subsequently adjusted to an electrical equivalent circuit. Independent observation of the circuit elements and their direct physical interpretation is useful to confirm the assumptions made with the Cole model parameters. The results support that the dynamics observed in R_0 are compatible with the changes produced in the membrane due to the formation of pores. Furthermore, the analysis demonstrates the hypothesis that the changes in the extracellular composition have greater impact than those of the intracellular space explaining the behaviour of R_∞.

The information obtained from the present multifrequency measurements supports the fact that the acquisition of a complete spectra instead of single frequency measurements enables more information about the system to be extracted. The present results demonstrate how fast EIS measurements during an electroporation procedure constitutes a reliable and alternative method for monitoring online the changes produced in the sample under treatment. This conclusion has considerable potential for *in vivo* applications where the control of tissue permeabilization during pulse delivery is critical for achieving the desired effect [33, 61, 62].

Acknowledgments

This research was supported by the COST TD1104 Action in the framework of the Short Term Scientific Missions (STSM). This work was also supported by CNRS, University Paris-Sud and IGR within the scope of the EBAM European Associated Laboratory (LEA).

Vitae

Tomás García-Sánchez obtained his degree in Telecommunication Engineering in 2010 from the Universitat Politècnica de València (UPV), Spain, his M.Sc in Biomedical Engineering in 2010 from a consortium between the Universitat Politècnica de València and the Universitat de València (UPV-UV). In April 2015, he obtained his Ph.D degree in Biomedical Engineering at the Universitat Politècnica de Catalunya (UPC), Barcelona, Spain. His research interests are focused on the study and design of microelectrode structures for bioelectric interfaces with a main application to electroporation and bioimpedance spectroscopy measurements.

Figure 9:

Javier Rosell-Ferrer was born in Barcelona, Spain, in June 1959. He received his Ingeniero de Telecomunicación degree and his doctorate in Ingeniero de Telecomunicación from the Polytechnic University of Catalunya (UPC), Barcelona, Spain, in 1983 and 1989, respectively. He is currently a Professor with the Department of Electronic Engineering, UPC, and is also with the Biomedical Research Center, UPC. His current research interests are focused on non-invasive measurement methods in sports, medical and biological fields based on bio-electrical impedance and magnetic induction spectroscopy.

Figure 10:

Ramon Bragós received the Telecommunication Engineer degree (1991) and the Eng. D.degree (1997) from the Technical University of Catalonia (UPC). From 1991 to 1998 was assistant professor and since 1998 has been associate professor at the Electronic Engineering Department, conducting his research with the Electronic and Biomedical Instrumentation research group. His research area is focused on biomedical and biotechnological instrumentation, with emphasis on electrical impedance spectroscopy applications.

Figure 11:

Lluis M. Mir graduated from the Ecole Normale Supérieure in Paris and obtained Ph.D in Toulouse in 1983. A CNRS researcher, he is the Director of the Laboratory of Vectorology and Anticancer Therapies (UMR 8203 CNRS and Université Paris-Saclay at Gustave Roussy, Villejuif, France). In 2010 he founded the European Associated Laboratory for the Applications of Electric Pulses in Biology and Medicine, which he co-directs with Pr. D. Miklavcic. He is also adjunct professor and honorary senator of the University of Ljubljana, and has been visiting professor at Berkeley, Bielefeld and Jerusalem Universities. He has coordinated research projects at French and European levels (5th and 6th FP), published 195 scientific articles and 21 book chapters (H index = 57), and has won several awards. He was President of the European Bioelectromagnetics Association (2012-2014). His main interests lie in the fields of membrane electropermeabilization in vitro and in vivo, especially with regard to the transfer of antitumor drugs after tumor cells electroporation (electrochemotherapy) and to the electrotransfer of genes (electrogenetherapy) to healthy and malignant tissues.

Figure 12:

Isabelle Leray obtained her master's degree in Cellular and Molecular Biology in 2005 from the University Montpellier II, France. She has co-authored 6 articles. She is currently employed as "assistante ingénieur" at the Laboratory of Vectorology and Anticancer Therapies of the CNRS and University Paris-Saclay at Gustave Roussy, Villejuif, France. She is working on different projects related to the mechanisms of cell electropermeabilization and on the cellular effects of microsecond or nanosecond electric pulses.

Figure 13:

Antoine AZAN received his engineering degree in Electronics in 2007 from the Institut National Polytechnique de Grenoble (INPG), Grenoble, France. After 4 years working as a radiofrequency designer for Thales Communication, he decided to pursue a university career. In 2011, he received a Master degree in Applied Physics from the Ecole Normale Supérieure de Cachan (ENS Cachan). In 2012, he received a Master 2 specialized in Physics/Biology interface from the University Paris Sud. Since October 2013, he has been working on his Ph.D in the UMR8203, research unit of CNRS and University Paris-Saclay at Gustave Roussy, Villejuif, France. His research interests are centered on the determination of the biochemical composition of biological samples exposed to intense electric pulses by non-invasive optical tools such as Raman spectroscopy and coherent anti-stokes Raman scattering microscopy.

Figure 14:

References

[1] J. Teissie, M. Golzio, M. P. Rols, Mechanisms of cell membrane electropermeabilization: A minireview of our present (lack of ?) knowledge, Biochimica et Biophysica Acta (BBA) - General Subjects 1724 (3) (2005) 270–280.

[2] L. M. Mir, Therapeutic perspectives of in vivo cell electropermeabilization, Bioelectrochemistry 53 (1) (2001) 1–10.

[3] F. M. Andre, L. M. Mir, Nucleic acids electrotransfer in vivo: mechanisms and practical aspects, Curr Gene Ther 10 (4) (2010) 267–80.

[4] J. Gehl, Electroporation for drug and gene delivery in the clinic: doctors go electric, Methods Mol Biol 423 (2008) 351–9.

[5] D. Miklavčič, G. Serša, E. Brecelj, J. Gehl, D. Soden, G. Bianchi, P. Ruggieri, C. R. Rossi, L. G. Campana, T. Jarm, Electrochemotherapy: technological advancements for efficient electroporation-based treatment of internal tumors, Medical & Biological Engineering & Computing 50 (12) (2012) 1213–1225.

[6] R. Davalos, L. Mir, B. Rubinsky, Tissue ablation with irreversible electroporation, Annals of Biomedical Engineering 33 (2) (2005) 223–231.

[7] S. Toepfl, V. Heinz, D. Knorr, Applications of Pulsed Electric Fields Technology for the Food Industry, Food Engineering Series, Springer US, 2006, Ch. 7, pp. 197–221.

[8] J. C. Weaver, Y. A. Chizmadzhev, Theory of electroporation: A review, Bioelectrochemistry and Bioenergetics 41 (2) (1996) 135–160.

[9] M. Tarek, Membrane electroporation: A molecular dynamics simulation, Biophysical Journal 88 (6) (2005) 4045–4053.

[10] R. W. Glaser, S. L. Leikin, L. V. Chernomordik, V. F. Pastushenko, A. I. Sokirko, Reversible electrical breakdown of lipid bilayers: formation and evolution of pores, Biochimica et Biophysica Acta (BBA) - Biomembranes 940 (2) (1988) 275–287.

[11] M. Hibino, M. Shigemori, H. Itoh, K. Nagayama, K. Kinosita Jr, Membrane conductance of an electroporated cell analyzed by submicrosecond imaging of transmembrane potential, Biophysical Journal 59 (1) (1991) 209–220.

[12] M. Bier, S. M. Hammer, D. J. Canaday, R. C. Lee, Kinetics of sealing for transient electropores in isolated mammalian skeletal muscle cells, Bioelectromagnetics 20 (3) (1999) 194–201.

[13] T. Griese, S. Kakorin, E. Neumann, Conductometric and electrooptic relaxation spectrometry of lipid vesicle electroporation at high fields, Physical Chemistry Chemical Physics 4 (7) (2002) 1217–1227.

[14] K. Kinosita Jr, T. Y. Tsong, Voltage-induced conductance in human erythrocyte membranes, Biochimica et Biophysica Acta (BBA) - Biomembranes 554 (2) (1979) 479–497.

[15] R. J. O'Neill, L. Tung, Cell-attached patch clamp study of the electropermeabilization of amphibian cardiac cells, Biophysical Journal 59 (5) (1991) 1028–1039.

[16] K. Kitamura, B. Judkewitz, M. Kano, W. Denk, M. Hausser, Targeted patch-clamp recordings and single-cell electroporation of unlabeled neurons in vivo, Nat Methods 5 (1) (2008) 61–7.

[17] M. Pavlin, D. Miklavcic, Effective conductivity of a suspension of permeabilized cells: A theoretical analysis, Biophysical Journal 85 (2) (2003) 719–729.

[18] A. L. Garner, C. Nianyong, Y. Jing, J. Kolb, R. J. Swanson, K. C. Loftin, S. J. Beebe, R. P. Joshi, K. H. Schoenbach, Time domain dielectric spectroscopy measurements of hl-60 cell suspensions after microsecond and nanosecond electrical pulses, Plasma Science, IEEE Transactions on 32 (5) (2004) 2073–2084.

[19] R. V. Davalos, D. M. Otten, L. M. Mir, B. Rubinsky, Electrical impedance tomography for imaging tissue electroporation, IEEE Trans Biomed Eng 51 (5) (2004) 761–7.

[20] A. Ivorra, B. Al-Sakere, B. Rubinsky, L. M. Mir, In vivo electrical conductivity measurements during and after tumor electroporation: conductivity changes reflect the treatment outcome, Phys Med Biol 54 (19) (2009) 5949–63.

[21] J. A. Stolwijk, C. Hartmann, P. Balani, S. Albermann, C. R. Keese, I. Giaever, J. Wegener, Impedance analysis of adherent cells after in situ electroporation: Non-invasive monitoring during intracellular manipulations, Biosensors and Bioelectronics 26 (12) (2011) 4720–4727.

[22] P. M. Ghosh, C. R. Keese, I. Giaever, Monitoring electropermeabilization in the plasma membrane of adherent mammalian cells, Biophysical Journal 64 (5) (1993) 1602–1609.

[23] U. Pliquett, R. Langer, J. C. Weaver, Changes in the passive electrical properties of human stratum corneum due to electroporation, Biochimica et Biophysica Acta (BBA) - Biomembranes 1239 (2) (1995) 111–121.

[24] E. Pasqualotto, A. Ferrario, M. Scaramuzza, A. De Toni, M. Maschietto, Monitoring electropermeabilization of adherent mammalian cells through electrochemical impedance spectroscopy, Procedia Chemistry 6 (0) (2012) 79–88.

[25] A. Silve, A. Guimerà Brunet, B. Al-Sakere, A. Ivorra, L. M. Mir, Comparison of the effects of the repetition rate between microsecond and nanosecond pulses: Electropermeabilization-induced electrodesensitization?, Biochimica et Biophysica Acta (BBA) - General Subjects 1840 (7) (2014) 2139–2151.

[26] Y. Yuxiang, K. Minhang, L. Yong, W. Jian, Y. Jing, G. Zonghai, Design of a wideband excitation source for fast bioimpedance spectroscopy, Measurement Science and Technology 22 (1) (2011) 013001.

[27] R. Bragos, R. Blanco-Enrich, O. Casas, J. Rosell, Characterisation of dynamic biologic systems using multisine based impedance spectroscopy, in: Instrumentation and Measurement Technology Conference, 2001. IMTC 2001. Proceedings of the 18th IEEE, Vol. 1, 2001, pp. 44–47 vol.1.

[28] U. F. Pliquett, K. H. Schoenbach, Changes in electrical impedance of biological matter due to the application of ultrashort high voltage pulses,

Dielectrics and Electrical Insulation, IEEE Transactions on 16 (5) (2009) 1273–1279.

[29] B. Sanchez, G. Vandersteen, R. Bragos, J. Schoukens, Optimal multisine excitation design for broadband electrical impedance spectroscopy, Measurement Science and Technology 22 (11) (2011) 115601.

[30] L. Raptis, K. L. Firth, Electroporation of adherent cells in situ, DNA Cell Biol 9 (8) (1990) 615–21.

[31] T. García-Sánchez, M. Guitart, J. Rosell-Ferrer, A. Gómez-Foix, R. Bragós, A new spiral microelectrode assembly for electroporation and impedance measurements of adherent cell monolayers, Biomedical Microdevices 16 (4) (2014) 575–590.

[32] E. Fattori, N. La Monica, G. Ciliberto, C. Toniatti, Electro-gene-transfer: a new approach for muscle gene delivery, Somat Cell Mol Genet 27 (1-6) (2002) 75–83.

[33] D. Cukjati, D. Batiuskaite, F. Andre, D. Miklavcic, L. M. Mir, Real time electroporation control for accurate and safe in vivo non-viral gene therapy, Bioelectrochemistry 70 (2) (2007) 501–7.

[34] B. Sanchez, R. Bragos, Fast Electrical Impedance Spectroscopy for Moving Tissue Characterization Using Bilateral QuasiLogarithmic Multisine Bursts Signals, Vol. 22 of IFMBE Proceedings, Springer Berlin Heidelberg, 2009, Ch. 259, pp. 1084–1087.

[35] H. P. Schwan, C. D. Ferris, Four-electrode null techniques for impedance measurement with high resolution, Review of Scientific Instruments 39 (4) (1968) 481–485.

[36] C. Zu-yao, G. A. M. Pop, G. C. M. Meijer, A comparison of two- and four-electrode techniques to characterize blood impedance for the frequency range of 100 hz to 100 mhz, Biomedical Engineering, IEEE Transactions on 55 (3) (2008) 1247–1249.

[37] E. Sarró, M. Lecina, A. Fontova, C. Solà, F. Gòdia, J. J. Cairó, R. Bragós, Electrical impedance spectroscopy measurements using a

four-electrode configuration improve on-line monitoring of cell concentration in adherent animal cell cultures, Biosensors and Bioelectronics 31 (1) (2012) 257–263.

[38] B. Sanchez, E. Louarroudi, R. Bragos, R. Pintelon, Harmonic impedance spectra identification from time-varying bioimpedance: theory and validation, Physiological Measurement 34 (10) (2013) 1217.

[39] J. Z. Bao, C. C. Davis, R. E. Schmukler, Impedance spectroscopy of human erythrocytes: system calibration, and nonlinear modeling, Biomedical Engineering, IEEE Transactions on 40 (4) (1993) 364–378.

[40] H. P. Schwan, Electrode polarization impedance and measurements in biological materials, Annals of the New York Academy of Sciences 148 (1) (1968) 191–209.

[41] I. Paul Ben, S. T. Mark, C. Andreas, L. Evgeniya, F. Yuri, Electrode polarization in dielectric measurements: a review, Measurement Science and Technology 24 (10) (2013) 102001.

[42] E. T. McAdams, J. Jossinet, Nonlinear transient response of electrode—electrolyte interfaces, Medical and Biological Engineering and Computing 38 (4) (2000) 427–432.

[43] E. A. Brown, J. D. Ross, R. A. Blum, N. Yoonkey, B. C. Wheeler, S. P. DeWeerth, Stimulus-artifact elimination in a multi-electrode system, Biomedical Circuits and Systems, IEEE Transactions on 2 (1) (2008) 10–21.

[44] B.-Y. Chang, S.-M. Park, Integrated description of electrode/electrolyte interfaces based on equivalent circuits and its verification using impedance measurements, Analytical Chemistry 78 (4) (2005) 1052–1060.

[45] D. R. Merrill, M. Bikson, J. G. R. Jefferys, Electrical stimulation of excitable tissue: design of efficacious and safe protocols, Journal of Neuroscience Methods 141 (2) (2005) 171–198.

[46] L. A. Geddes, Historical evolution of circuit models for the electrode-electrolyte interface, Annals of Biomedical Engineering 25 (1) (1997) 1–14.

[47] H. Kalvoy, G. K. Johnsen, O. G. Martinsen, S. Grimnes, New method for separation of electrode polarization impedance from measured tissue impedance, Open Biomed Eng J 5 (2011) 8–13.

[48] S. Kun, B. Ristic, R. A. Peura, R. M. Dunn, Real-time extraction of tissue impedance model parameters for electrical impedance spectrometer, Medical & Biological Engineering & Computing 37 (4) (1999) 428–432.

[49] H. Fricke, S. Morse, The electric resistance and capacity of blood for frequencies between 800 and 4(1/2) million cycles, J Gen Physiol 9 (2) (1925) 153–67.

[50] A. Ivorra, Tissue Electroporation as a Bioelectric Phenomenon: Basic Concepts, Series in Biomedical Engineering, Springer Berlin Heidelberg, 2010, Ch. 2, pp. 23–61.

[51] H. Shagoshtasbi, L. Yi-Kuen, A new equivalent circuit model for micro electroporation systems, in: Nano/Micro Engineered and Molecular Systems (NEMS), 2011 IEEE International Conference on, 2011, pp. 662–665.

[52] Y. Huang, B. Rubinsky, Micro-electroporation: Improving the efficiency and understanding of electrical permeabilization of cells, Biomedical Microdevices 2 (2) (1999) 145–150.

[53] L. F. Cima, L. M. Mir, Macroscopic characterization of cell electroporation in biological tissue based on electrical measurements, Applied Physics Letters 85 (19) (2004) 4520–4522.

[54] D. A. Zaharoff, J. W. Henshaw, B. Mossop, F. Yuan, Mechanistic analysis of electroporation-induced cellular uptake of macromolecules, Exp Biol Med (Maywood) 233 (1) (2008) 94–105.

[55] M. Pavlin, M. Kanduser, M. Rebersek, G. Pucihar, F. X. Hart, R. Magjarevic, D. Miklavcic, Effect of cell electroporation on the conductivity of a cell suspension, Biophys J 88 (6) (2005) 4378–90.

[56] H. He, D. C. Chang, Y.-K. Lee, Nonlinear current response of micro electroporation and resealing dynamics for human cancer cells, Bioelectrochemistry 72 (2) (2008) 161–168.

[57] M. Khine, C. Ionescu-Zanetti, A. Blatz, L.-P. Wang, L. P. Lee, Single-cell electroporation arrays with real-time monitoring and feedback control, Lab on a Chip 7 (4) (2007) 457–462.

[58] M. Leguèbe, A. Silve, L. M. Mir, C. Poignard, Conducting and permeable states of cell membrane submitted to high voltage pulses: Mathematical and numerical studies validated by the experiments, Journal of Theoretical Biology 360 (0) (2014) 83–94.

[59] M. Pavlin, V. Leben, D. Miklavčič, Electroporation in dense cell suspension—theoretical and experimental analysis of ion diffusion and cell permeabilization, Biochimica et Biophysica Acta (BBA) - General Subjects 1770 (1) (2007) 12–23.

[60] H. Wolf, M. P. Rols, E. Boldt, E. Neumann, J. Teissie, Control by pulse parameters of electric field-mediated gene transfer in mammalian cells, Biophysical Journal 66 (2, Part 1) (1994) 524–531.

[61] J. Gehl, L. M. Mir, Determination of optimal parameters for in vivo gene transfer by electroporation, using a rapid in vivo test for cell permeabilization, Biochemical and Biophysical Research Communications 261 (1999) 377–380.

[62] Y. Granot, A. Ivorra, E. Maor, B. Rubinsky, In vivo imaging of irreversible electroporation by means of electrical impedance tomography, Phys Med Biol 54 (16) (2009) 4927–43.

Highlights

- EIS measurements based on multisine excitations are shown to be a feasible method to capture fast electroporation dynamics.
- Multifrequency information reveals a dual dynamic membrane resealing mechanism.
- Impedance models are demonstrated to help in the study of electroporation.
- EIS measurements provide simultaneous information about membrane poration and about the collateral conductivity variations caused by diffusion of ions.